Inorganic Chemistry

Article

pubs.acs.org/IC

Kinetic Studies of the $[NpO_2(CO_3)_3]^{4-}$ Ion at Alkaline Conditions Using ^{13}C NMR

Adele F. Panasci,[†,§] Stephen J. Harley,[§] Mavrik Zavarin,[§] and William H. Casey*[,†,‡]

[†]Department of Chemistry and [‡]Department of Earth and Planetary Sciences, University of California, Davis, One Shields Avenue, Davis, California 95616, United States

[§]Lawrence Livermore National Laboratory, 7000 East Avenue, Livermore, California 94550, United States

Supporting Information

ABSTRACT: Carbonate ligand-exchange rates on the $[NpO_2(CO_3)_3]^{4-}$ ion were determined using a saturation-transfer ^{13}C nuclear magnetic resonance (NMR) pulse sequence in the pH range of $8.1 \leq pH \leq 10.5$. Over the pH range $9.3 \leq pH \leq 10.5$, which compares most directly with previous work of Stout et al.,[1] we find an average rate, activation energy, enthalpy, and entropy of $k_{ex}^{298} = 40.6(\pm4.3)\ s^{-1}$, $E_a = 45.1(\pm3.8)$ kJ mol^{-1}, $\Delta H^{\ddagger} = 42.6(\pm3.8)$ kJ mol^{-1}, and $\Delta S^{\ddagger} = -72(\pm13)$ J mol^{-1} K^{-1}, respectively. These activation parameters are similar to the Stout et al. results at pH 9.4. However, their room-temperature rate at pH 9.4, $k_{ex}^{298} = 143(\pm1.0)\ s^{-1}$, is ∼3 times faster than what we experimentally determined at pH 9.3: $k_{ex}^{298} = 45.4(\pm5.3)\ s^{-1}$. Our rates for $[NpO_2(CO_3)_3]^{4-}$ are also faster by a factor of ∼3 relative to the isoelectronic $[UO_2(CO_3)_3]^{4-}$ as reported by Brucher et al.[2] of $k_{ex}^{298} = 13(\pm3)\ s^{-1}$. Consistent with results for the $[UO_2(CO_3)_3]^{4-}$ ion, we find evidence for a proton-enhanced pathway for carbonate exchange for the $[NpO_2(CO_3)_3]^{4-}$ ion at pH < 9.0.

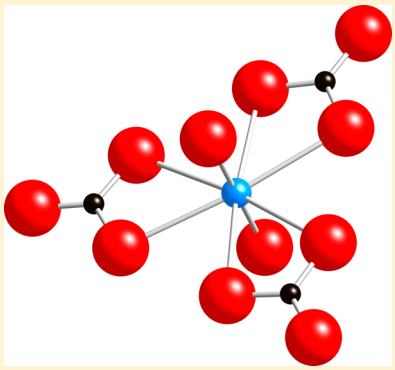

INTRODUCTION

The future of the nuclear industry depends on a defendable understanding of environmental risks associated with nuclear accidents and nuclear waste storage. Assessing the safety of storage facilities relies on accurate models that predict how actinide species migrate through engineered barriers, soil, and groundwater.[3] However, modeling the transport of these species, particularly the actinide elements, is difficult due to multiple oxidation states that may be present in natural waters, the presence of complexing ligands, their potential to form colloids, and their interactions with mineral surfaces.[4] Reactive-transport models rely on data from experiments to accurately address these many interactions, but the lack of such data remains a barrier to building effective actinide reactive-transport models. Particularly valuable are the highly constrained experiments that describe simple molecular processes, like ligand exchanges, where the reaction scale can be compared directly with ab initio and molecular-dynamic simulations.

The neptunium actinide is particularly troublesome due to its long half-life, 2.14×10^6 years for the ^{237}Np isotope, its high solubility at conditions typical of natural groundwaters, and its high toxicity. Neptunium in water can exist in oxidation states ranging from (III) to (VII), with the pentavalent state being the most stable, while in the pentavalent and hexavalent states neptunium exists with opposing axial 'yl' oxygens having a high bond order and equatorial bound waters as NpO_2^+ and NpO_2^{2+}, respectively. There has been an emphasis on studying the chemical behavior of neptunium in acidic to neutral conditions even though nuclear waste is likely to be stored in an alkaline environment.[8−15] Although the hydrated neptunium species are less soluble at high pH values, common ligands in the environment, such as carbonate, can bind to neptunium under these conditions and substantially increase its solubility.[16]

Previous thermodynamic studies showed that in the presence of carbonate and bicarbonate Np(VI) dominantly exists as the monomeric species $[NpO_2(CO_3)]^0$, $[NpO_2(CO_3)_2]^{2-}$, and $[NpO_2(CO_3)_3]^{4-}$ or as the trimeric species $[(NpO_2)_3(CO_3)_6]^{6-}$.[17−23] Even at pH values where bicarbonate is at higher concentration than carbonate, monodentate bicarbonate complexes are not found.[18] At high ionic strength and pH less than 7.7, the trimeric species, $[(NpO_2)_3(CO_3)_6]^{6-}$, dominates, while at higher pH conditions and ratios of NpO_2^{2+}:CO_3^{2-} of 1:3 or greater the monomeric $[NpO_2(CO_3)_3]^{4-}$ species (Figure 1) dominates.

Tait et al. used ^{13}C NMR spectroscopy to determine the speciation of the Np(VI)−carbonate solutions.[24] The monomeric $[NpO_2(CO_3)_3]^{4-}$ species exhibits a single ^{13}C NMR peak attributable to bound carbonate with a chemical shift around ∼80 ppm (Figure 2), while the trimeric species exhibits two peaks at approximately 8 and −89 ppm, again corresponding to bound ligands.

In this paper we extend the work by Stout et al.[1] by revisiting the kinetic behavior of carbonate ligand exchange on the $[NpO_2(CO_3)_3]^{4-}$ ion. Stout et al. reported activation parameters for two pH conditions. These parameters are listed in Table 1. They report the rate of ligand exchange of $k_{ex}^{298} = 143(\pm1.0)$ and $64.7(\pm3.3)\ s^{-1}$ at a pH values of 9.4 and 10.0,

Received: February 10, 2014
Published: April 1, 2014

   dx.doi.org/10.1021/ic500314v | Inorg. Chem. 2014, 53, 4202−4208

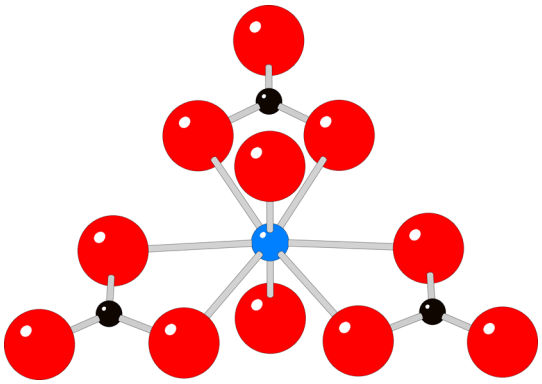

Figure 1. $[NpO_2(CO_3)_3]^{4-}$ ion. Np(VI) is light blue, oxygen red, and carbon black. Two opposing "yl" oxygens are in the axial positions, while the three, bidentate carbonate ligands are in the equatorial plane.

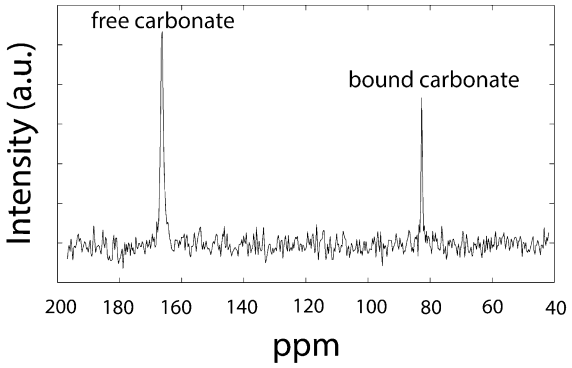

Figure 2. ^{13}C NMR spectra of sample 5 (see Table 2). Peaks are well separated and indicate slow exchange on the NMR time scale.

Table 1. Activation Parameters Reported by Stout et al.[1] at 25 °C

pH	E_a (kJ mol^{-1})	k_{ex}^{298} (s^{-1})	$\Delta H^{\ddagger}$(kJ mol^{-1})	$\Delta S^{\ddagger}$(J mol^{-1} K^{-1})
9.4	43.8 ± 6.3	143 ± 1.0	41.8 ± 6.3	−65 ± 21
10.0	43.8 ± 6.7	64.7 ± 3.3	41.8 ± 6.6	−71 ± 22

respectively.[1] They employed relatively high concentrations of metal [Total Np(VI) = 0.10 M] and ligand [Total carbonate = 0.70 M] and ionic strength of 1.0 M.

With these solutions, they used the line-broadening method described by Swift and Connick[25] in which NMR peak width and chemical shift differences are assigned to the free carbonate ion with and without the paramagnetic metal, in this case Np(VI). This method is most commonly used when the signal for the reactive species is unobservable due to paramagnetic broadening and fast exchange, such as when ^{17}O exists in the hydration shell of paramagnetic monomer ions (e.g., $[Fe(OH_2)_6]^{3+}$,[19,26,27]) and exchanges with bulk water. The rate of exchange from the solvation shell is inferred from the effect on the bulk solution ^{17}O peak. ^{13}C NMR spectra for the $[NpO_2(CO_3)_3]^{4-}$ ion carbonate solution contain two well-separated peaks, one for the free carbonate (166 ppm) and one for the bound carbonate (84 ppm), which is consistent with the spectra reported by Stout et al. and Tait et al.[1,24] (Figure 2). The presence of two individual signals, one assignable to the bound carbonate ligand and one assignable to free carbonate, indicate that ligand exchange between bound and free carbonate is slow on the NMR time scale.

We found the free and bound carbonate peaks to be sufficiently well separated to permit selective-excitation experiments that yield kinetic information about the rates of substitution directly, which is a second means of estimating rate coefficients that is independent of assumptions of the Swift−Connick method. This method also allows us to conduct experiments at total Np(VI) and carbonate concentrations that are lower than those of Stout et al., thus complementing their work. The chemical shift difference, however, is small enough (∼12 kHz) that we could not selectively excite a peak using a conventional 180° long pulse. Instead, we adapted an approach we previously employed to study the $[UO_2(CO_3)_3]^{4-}$ species, which also has close chemical shifts.[28] We conducted ^{13}C NMR saturation-transfer experiments on the $[NpO_2(CO_3)_3]^{4-}$ion, which is isoelectronic to the $[UO_2(CO_3)_3]^{4-}$ species, and determined carbonate ligand-exchange parameters across a wider pH range than the experiments described in the Stout et al. paper.

EXPERIMENTAL SECTION

Caution: ^{237}Np is a radioactive isotope and an α-emitter. It should be handled in dedicated facilities with appropriate equipment for radioactive materials to avoid health risks caused by radiation exposure.

Sample Preparation. A stock solution of Np(V) was prepared using the ^{237}Np column purification method of Snow et al.[29] The solution was washed and dried until the solid would not dissolve in water, heated to full dryness, and redissolved into a solution prepared from water of 18-Megaohm resistance that was made slightly acidic with dilute perchloric acid, such that perchlorate would be the counterion. The neptunium concentration of the solution was established by liquid-scintillation counting. The resulting solution was a mix of oxidation states, which we adjusted using a Wavenow USB potentiostat. The potentiostat had a three-electrode array with a Pt-wire working electrode that was separated from a Pt-wire counter electrode by a Vycor frit. The reference electrode was an Ag/AgCl microelectrode.

Solutions were kept under electrolysis at +1.35 V[30−32] until the characteristic UV−vis−NIR peaks of Np(IV) and Np(V) at 960 and 980 nm, respectively, disappeared and the characteristic peak for Np(VI), 1230 nm, became prominent (Figure 3). Once the solution was electrochemically treated to convert neptunium to Np(VI), the solvent was evaporated away and the solid was then redissolved in sodium−carbonate solution that had been enriched with ^{13}C (98%). Aliquots of this stock solution were used to make subsamples for experiment containing 5−15 mM Np(VI) and 20−60 mM carbonate, ensuring that the carbonate concentration was at least four times that of the Np(VI) and that the tris-carbonato species formed. The pH was measured using an Ingold microelectrode and adjusted using dilute perchloric acid or sodium hydroxide. Once the sodium carbonate was added, the UV−vis−NIR of the solution was taken again, Figure 4, to confirm formation of monomeric $[NpO_2(CO_3)_3]^{4-}$; these results were consistent with the spectra reported by Ikeda-Ohno et al.[17] The solution compositions that were employed in experiments are reported in Table 2.

All experiments were performed within 1 week of solution preparation, and we found no evidence of sample degradation during this time. No precipitate formed in any samples for which rate data are reported, although samples at pH ≥ 10.6 formed a precipitate within 2 h of preparation. The pH values of the samples were measured before and after the NMR experiments to verify that changes in temperature did not alter the pH of the solution via hydrolysis; in all cases the pH varied no more than 0.1 pH units. The pH of the sample solutions were prevented from dropping to pH < 8 to ensure that no trimeric species formed. Similarly, NMR spectra were collected on each sample to confirm that no trimeric complex formed, which would have been evident as ^{13}C NMR peaks at 8 and −89 ppm. The only Np(VI)

dx.doi.org/10.1021/ic500314v | Inorg. Chem. 2014, 53, 4202−4208

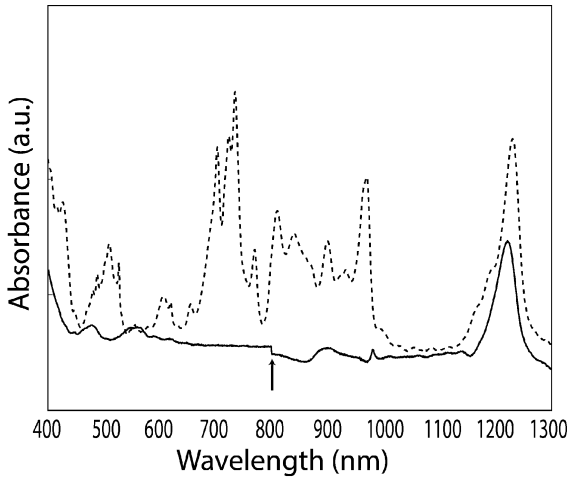

Figure 3. UV−vis−NIR spectra of 10 mM neptunium stock solution before and after electrochemistry. The peak characteristic for Np(VI) is at 1230 nm. Dashed line shows the UV−vis−NIR spectrum before electrolysis when Np(IV), Np(V), and Np(VI) are present. Solid line is after electrolysis when the solution is nearly pure in Np(VI). The discontinuity in adsorption at 800 nm, indicated by the vertical arrow, is caused by mechanical changes in the light source in the instrument and does not indicate a real chemical change.

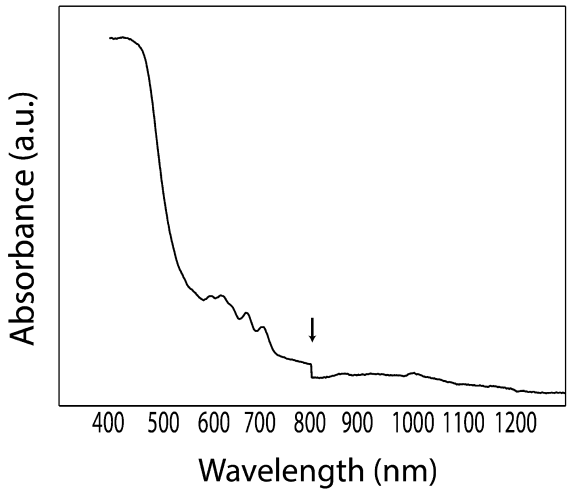

Figure 4. UV−vis−NIR of a solution after purification and after sodium carbonate had been added (sample 5; see Table 2). Absorption between 400 and 700 nm and the minor peaks at 550−750 nm are characteristic of Np(VI). The lack of absorption around 800 nm indicates the absence of Np(V)−carbonate species. The discontinuity in adsorption at 800 nm, indicated by the vertical arrow, is caused by mechanical changes in the light source.

Table 2. Composition of Aqueous Solutions Used for Saturation-Transfer Experiments

	[neptunium] (mM)	[carbonate] (mM)	pH	ionic strength (M)
sample 1	12	54.5	10.5	0.21
sample 2	12	54.5	8.8	0.21
sample 3	10	52	9.3	0.21
sample 4	8	32	10.1	0.15
sample 5	7.2	50	10.1	0.20
sample 6	10	50	8.1	0.18
sample 7	10	50	8.55	0.18

species detectable in our solutions was the monomeric $[NpO_2(CO_3)_3]^{4-}$ complex.

NMR Spectroscopy. Nuclear magnetic resonance (NMR) measurements were carried out using a Bruker Avance DRX 600 MHz (14.1 T, ^{13}C 151.01 MHz) spectrometer equipped with a 5 mm broad-band probe. Because of the inherent danger of neptunium, the sample was doubly contained in the NMR using a Wilmad-Labglass Pyrex coaxial system for toxic samples. ^{13}C spectra were acquired using the previously described pulse sequence[28] consisting of three 90° hard-pulse excitations using 11.26 μs 90° pulse with a recycle delay of 0.5 s to ensure complete relaxation. A schematic of the pulse sequence and magnetization movement is shown in Figure 5.

For our experiments, the sweep width was set to 1000 ppm (150.8 kHz) and we collected between 100 and 200 scans, depending on the particular solution, in order to establish an adequate signal-to-noise ratio. Temperature was controlled using the Bruker Avance temperature controller, and experiments were collected over the temperature range of 293−340 K. The variation in the temperature reported by the Bruker system and the temperature inside the NMR sample tube was calibrated using neat ethylene glycol,[33,34] and the uncertainty in the temperature was determined to be ±0.2 K.

In this pulse program, the magnetization of both sites is initially tipped into the xy plane using a hard 90° pulse on the x axis. A calculated delay time, τ_{Prec}, is allowed to pass so magnetization that is not on resonance will rotate in the xy plane until the two signals are exactly 180° out of phase. Then, a hard 90° pulse is reapplied along the x axis to flip both signals, but one is inverted. A variable-time delay is then applied to allow mixing of the two magnetizations until a third hard 90° pulse is applied along the x axis to tip both magnetizations into the xy plane for detection. As the magnetization is transferred between the two sites, the intensity of the inverted peak will increase and that of the positive site will decrease (Figure 6) because of chemical exchange.

The system is modeled using the Bloch equations with the McConnell formalism for exchange (eqs 1 and 2)

$$\frac{dM_{z,free}(t)}{dt} = \frac{[M_{z,free}(t) - M^{eq}_{z,free}]}{T_{1,free}} + k_{bound}M_{z,bound}(t) - k_{free}M_{z,free}(t) \quad (1)$$

$$\frac{dM_{z,bound}(t)}{dt} = \frac{[M_{z,bound}(t) - M^{eq}_{z,bound}]}{T_{1,bound}} + k_{free}M_{z,free}(t) - k_{bound}M_{z,bound}(t) \quad (2)$$

where $M_{z,i}(t)$ and $M^{eq}_{z,i}$ are the magnitude of the z magnetization for species i as a function of time and equilibration, respectively, $T_{1,i}$ is the longitudinal relaxation rate of species i, and k_i is the rate constant for ligand exchange between the bound and the free state. Due to the law of detailed balance, $X_{free}k_{free} = X_{bound}k_{bound}$, where X_{free} and X_{bound} are the concentrations of the free and bound carbonate, respectively. Each peak was phased independently and then fit to a Lorenzian function, and the amplitude value for each peak was organized according to mixing time. The rate of exchange for the bound species, k_{bound}, was obtained by analytically solving the coupled differential equations above (Figure 7, see also the Supporting Information) and then fitting the solutions via least-squares minimization using a Levenberg−Marquardt algorithm. The T_1 values for the free and bound carbonate were also allowed to adjust in the optimization algorithm, but the resulting rate coefficients are insensitive to these values. Nevertheless, these optimized T_1 values for the free carbonate and the fitting uncertainties are reported in the Supporting Information.

The rates thus determined were plotted as a function of $1/T$ in order to derive activation parameters (k^{298}_{ex}, $\Delta H^{\ddagger}$, and $\Delta S^{\ddagger}$) via the Arrhenius equation (Figure 8, see also the Supporting Information). A Monte Carlo algorithm was used to assign uncertainties to the activation parameters. We created an array of 1000 randomly generated numbers having a mean value of the regressed rate and a standard deviation of the regression standard deviation for each

dx.doi.org/10.1021/ic500314v | Inorg. Chem. 2014, 53, 4202−4208

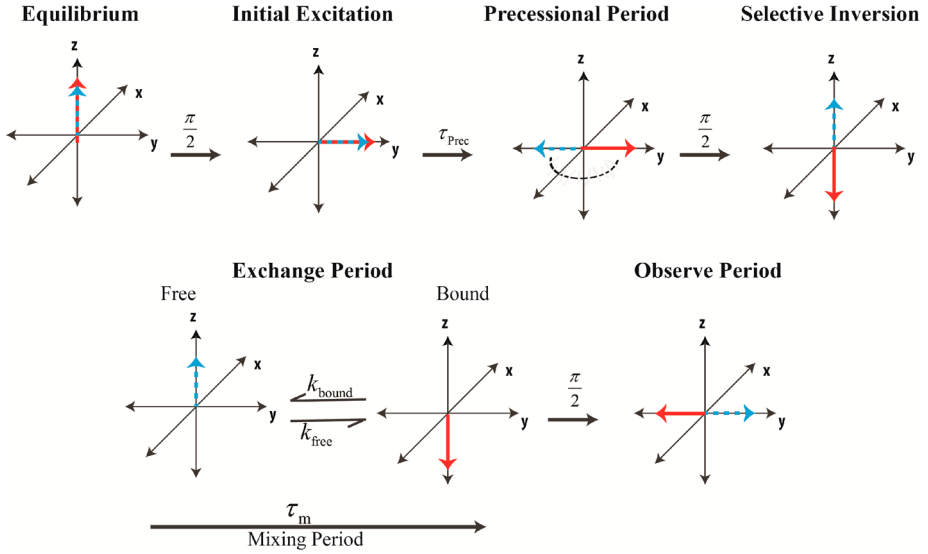

Figure 5. Saturation-transfer pulse sequence used to separate the signals from two closely spaced complexes. Solid arrow represents the magnetization of the species that is put on resonance, and dotted arrow represents the magnetization of the species not on resonance.[28]

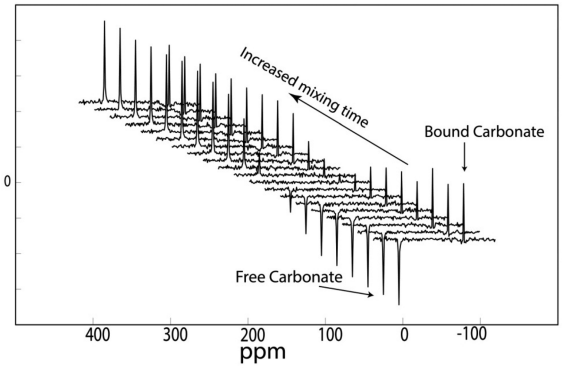

Figure 6. ^{13}C NMR spectra of a saturation-transfer experiment for sample 5 (see Table 2). Free carbonate peak is inverted, and the magnetization relaxes back along the z axis after an adjustable mixing time.

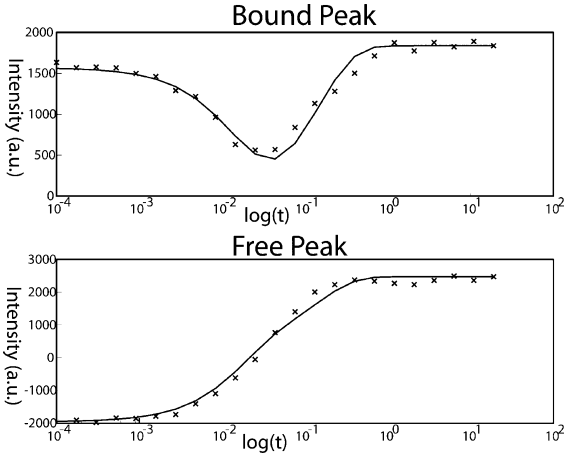

Figure 7. Magnetization-transfer experiment of $[NpO_2(CO_3)_3]^{4-}$ (aq) for sample 5 (7.2 mM neptunyl at 10.1 pH): (×) measurements; (—) the best fit to these data.

temperature. A single point of each temperature array was randomly chosen and linearly regressed to calculate the slope and intercept. This single-point process was repeated 1000 times. The mean and standard

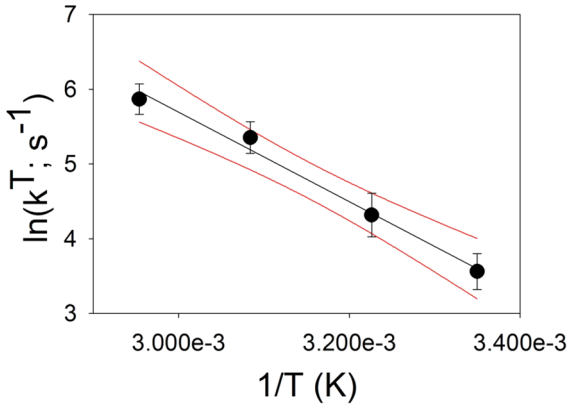

Figure 8. Plot of ln(k) vs $1/T$ for the exchange of carbonate in $[NpO_2(CO_3)_3]^{4-}$ for sample 1 (12 mM $[NpO_2(CO)_3]^{4-}$ solution at pH 10.5). Experimental results are shown by the dots, and the solid line is the best fit. Red lines indicate the 95% confidence interval.

deviation of these aggregated slopes and intercept values were then used to estimate the uncertainties in all activation parameters. We report these uncertainties in Table 3.

Banyai et al. extended the study of Brucher et al., who reported a first-order exchange reaction for the $[UO_2(CO_3)_3]^{4-}$ ion.[2,37] First-order kinetics were also reported for carbonate exchange of $[UO_2(CO_3)_3]^{5-}$ and $[PuO_2(CO_3)_3]^{4-}$ in solutions at high pH.[19,35] As we show (below), the first-order model adequately accounts for the experimental results[1] and is implicit in eqs 1 and 2.

RESULTS

Our data (Table 3) agree well with Stout et al.[1] (Table 1), who reported rates for only two samples at pH 9.4 and 10.0 and at different solution conditions. A proton-enhanced pathway at pH < 9 is apparently present (see below), making the results consistent with previous work on the isoelectronic and isostructural $[UO_2(CO_3)_3]^{4-}$ molecule. For samples between $9.3 \leq pH \leq 10.5$, there appears to be no strong correlation between the exchange rates and activation enthalpy, pH, or the concentration of Np(VI). If we reject the idea of a pH dependence of the rate for these samples, the average activation parameters at $9.3 \leq pH \leq 10.5$ are found to be k_{ex}^{298} =

dx.doi.org/10.1021/ic500314v | Inorg. Chem. 2014, 53, 4202−4208

Table 3. Experimental Activation Parameters

	$[NpO_2(CO_3)_3]^{4-}$ (mM)	pH	E_a (kJ mol^{-1})	k_{ex}^{298} (s^{-1})	$\Delta H^{\ddagger}$ (kJ mol^{-1})	$\Delta S^{\ddagger}$ (J mol^{-1} K^{-1})
sample 1	12	10.5	49.8 ± 9.2	35.2 ± 5.4	47.3 ± 7.2	−57 ± 24
sample 2	12	8.8	44.9 ± 11	53.1 ± 4.6	42.3 ± 8.7	−63 ± 17
sample 3	10	9.3	44.1 ± 9.4	45.4 ± 5.3	41.6 ± 6.9	−74 ± 26
sample 4	8	10.1	39.5 ± 11	37.5 ± 6.5	37.0 ± 8.9	−91 ± 30
sample 5	7.2	10.1	46.8 ± 10	44.1 ± 5.9	44.3 ± 8.0	−64 ± 27
sample 6	10	8.1	28.1 ± 12	157 ± 6.2	25.7 ± 9.1	−117 ± 30
sample 7	10	8.55	50.0 ± 8.9	93.3 ± 5.8	47.5 ± 6.4	−48 ± 22

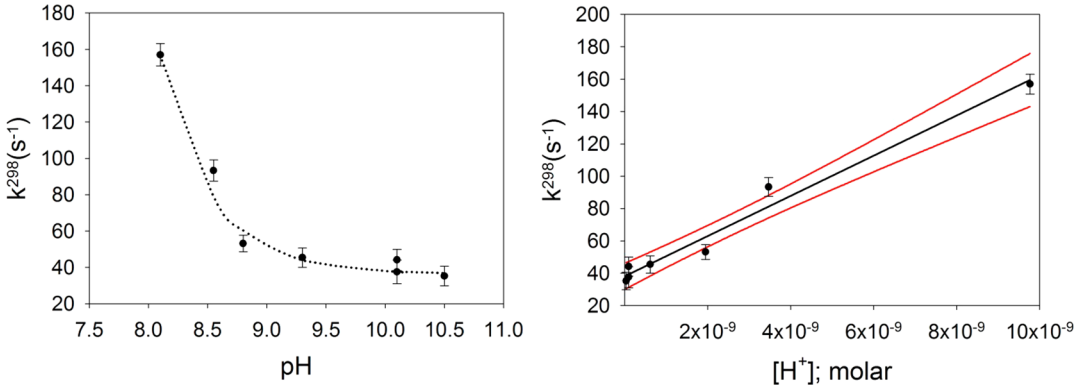

Figure 9. Experimental rate data plotted from Table 2 as a function of solution pH. Dotted line is the approximate location of a least-squares fit of eq 3 to the data, yielding k_1 = 36.3 s^{-1} and k_2 = 1.23 × 10^{10} M^{-1} s^{-1}, using γ_{H^+} = 0.81 to convert proton activities to concentrations. (Right) Data regressed against hydrogen-ion concentration, yielding a slope of 1.243(±0.04) × 10^{10} M^{-1} s^{-1} and an intercept of 38 s^{-1}(±3). The 95% confidence interval is shown as red lines.

40.6(±4.3) s^{-1}, E_a = 45.1(±3.8) kJ mol^{-1}, $\Delta H^{\ddagger}$ = 42.6(±3.8) kJ mol^{-1}, and $\Delta S^{\ddagger}$ = −72 (±13) J mol^{-1} K^{-1}. The precision of the measurements can be gauged by comparing the results for samples 4 and 5, which have similar concentrations and pH values. The difference in k_{ex}^{298} is ∼7 s^{-1}, and the difference in the enthalpy is ∼7 kJ mol^{-1}, which is close to the estimated uncertainties for a single measurement. These are also similar to the uncertainty values reported by Stout et al.[1] of ±3.3 s^{-1} and 6.7 kJ mol^{-1} for rate and enthalpy, respectively. Buffers were avoided in our study because of the possibility that they alter the speciation or kinetics. The similarity of our data to Stout et al.[1] indicates that the effects are negligible.

DISCUSSION

In the pH range 9.3 < pH < 10.5, where there is no evident proton enhancement, our data for carbonate exchange, expressed as k_{ex}^{298}, are consistent with, but lower than, those proposed by Stout et al.[1] by about a factor of 1.5−3.5. They reported rates of 143(±1.0) and 64.7(±3.3) s^{-1} for pH 9.4 and 10.0, respectively. We determined an average ligand exchange rate of 40.6(±4.3) s^{-1} at 9.3 ≤ pH ≤ 10.5. As we mentioned above, the rates determined by Stout et al[1] were obtained using the Swift−Connick[25] formalism which measures the broadening in the spectral line width as a result of the ligand exchange, while the rates we report were determined using the saturation-transfer technique, which directly measures the rate of magnetization exchange between the bound and free carbonate. Szabo and Grenthe[36] demonstrated that saturation-transfer experiments gave more accurate rate values than the line-broadening technique when the exchange is slow on the NMR time scale, resulting into two well-defined peaks, as is the case for the $[NpO_2(CO_3)_3]^{4-}$ system.

Banyai et al. determined that there are two pathways of carbonate ligand exchange on the $[UO_2(CO_3)_3]^{4-}$ ion.[37] The first pathway dominates at higher pH, is independent of pH, and is controlled by the unenhanced dissociation of the carbonate ligand from the complex, for which at pH > 8.7 they report k_{ex}^{298} = 13(±3) s^{-1} and $\Delta H^{\ddagger}$ and $\Delta S^{\ddagger}$ of 82(±11) kJ mol^{-1} and 50(±30) J mol^{-1} K^{-1}, respectively.[37] The second pathway depends on proton concentration, for which at pH < 8.6 they reported k_{ex}^{298} = 2.32(±0.03) × 10^9 s^{-1} M^{-1}. They calculated this rate using the following equation (eq 3)

$$k_2 = \frac{(k_{obs} - k_1)}{[H^+]} \quad (3)$$

We conducted experiments at pH < 9 specifically to search for evidence of a proton-enhanced pathway in the $[NpO_2(CO_3)_3]^{4-}$ complex. Using the values we obtained for the experiments at pH = 9.3 and 8.8 as indicating an unenhanced pathway, the presence of a proton-enhanced pathway would not be evident unless the rate coefficient, k_2, were greater than ∼1 × 10^{10} s^{-1} M^{-1}. Furthermore, one anticipates that the experimental activation enthalpy would be smaller to reflect a contribution from the enthalpy of protonation. Both of these phenomena should be observed as the proton-enhanced pathway becomes evident in the raw experimental data. For samples 6 (pH = 8.1) and 7 (pH = 8.55) we calculate k_2 ≈1.9 × 10^{10} and ∼1.5 × 10^{10} s^{-1} M^{-1}, respectively, from eq 3. For both samples, the experimental activation energies (and enthalpies) are significantly smaller than the values at pH > 9. The values of $\Delta H^{\ddagger}$ for all samples with pH ≥ 8.55 are 43.3(±4) kJ mol^{-1}. The values for samples 2 and 7 are indistinguishable from this average. However, our lowest pH sample, sample 6, exhibited $\Delta H^{\ddagger}$ = 25.7(±9) kJ mol^{-1}, which is significantly distinct from the higher pH results.

dx.doi.org/10.1021/ic500314v | Inorg. Chem. 2014, 53, 4202−4208

We therefore conclude that there is a proton-enhanced pathway for exchange of carbonate, as Banyai et al.[37] observed for the $[UO_2(CO_3)_3]^{4-}$ complex, and that it is evident only at pH < 8.6. The contribution of the proton-enhanced pathway is evident in Figure 9a and 9b.

There is understandable disagreement about the mechanisms of the carbonate ligand-exchange reaction, which must be at least a two-step process. Free carbonate (or bicarbonate) must associate with the ion and either exploit or induce a ring opening of an existing ligated bidentate carbonate. Once the ring opens, the incoming carbonate could bond via a unidentate oxygen and collapse into a ring when the leaving carbonate is gone.

What is not fully clear is whether there exists an intermediate state of aquated Np(VI) between the incoming and the outgoing carbonates. Elucidation of such detail is difficult because the evidence to constrain it consists of experimental entropies, which themselves must be composite parameters. Carbonate exchange in $[UO_2(CO_3)_3]^{4-}$, $[UO_2(CO_3)_3]^{5-}$, and $[PuO_2(CO_3)_3]^{4-}$ are reported as dissociative,[2,28,35] while Stout et al., as do we, reported negative activation entropies for both the U(VI) species and the Np(VI) species.[1] Stout et al. used these negative entropies to suggest a more associative mechanism between the complex and the incoming carbonate ligand.

To extend their work, we recently measured apparent activation volumes for both the proton-enhanced and pH-independent pathways using high-pressure NMR.[28] The net activation volumes for the $[UO_2(CO_3)_3]^{4-}$ proton-enhanced pathway and the pH-independent pathway were found to be positive, +6.6(±0.7) and +10.6(±0.7) cm^3 mol^{-1}, respectively.[28] These activation volumes correspond to a multistep reaction pathway and cannot be uniquely interpreted to indicate a mechanism of exchange, but an obvious question is whether these values are quantitatively similar for the nearly identical $[NpO_2(CO_3)_3]^{4-}$ ion. Addition of apparent activation volumes could couple to new methods of simulation of volume changes during the reaction and advance the field since the simulations would treat structurally very similar molecules.[38] Finally, we think that the overall similarity in reactivity between the Np(VI) and the U(VI) complexes is important to geochemical efforts, since the reactivities of transuranic elements are so poorly documented in natural systems.

■ ASSOCIATED CONTENT

Supporting Information

The Supporting Information contains model equations, spectral information, summaries of fitted parameters and fits to the NMR spectra.This material is available free of charge via the Internet at http://pubs.acs.org.

■ AUTHOR INFORMATION

Corresponding Author

*E-mail: whcasey@ucdavis.edu.

Notes

The authors declare no competing financial interest.

■ ACKNOWLEDGMENTS

The authors are particularly grateful for advice from Dr. David Clark of LANL and to Professor Thomas Albrecht-Schmitt for loan of ^{237}Np that helped us begin experiments with neptunium. We would also like to thank Pihong Zhao for the advice on neptunium purification and Christopher Colla for his work on the figure of the neptunyl complex. This work was supported by the Subsurface Biogeochemical Research Program of the U.S. Department of Energy's Office of Biological and Environmental Research; Prepared by LLNL under Contract DE-AC52-07NA27344. It was also supported by the Office of Basic Energy Science of the U.S. Department of Energy as part of the Materials Science of Actinides Energy Frontier Research Center (DE-SC0001089). This work was supported by the Lawrence Livermore National Laboratory Lawrence Scholar Fellowship.

■ REFERENCES

(1) Stout, B. E.; Choppin, G. R.; Sullivan, J. C.*Transuranium elements: a half century*; American Chemical Society: Washington, D.C., 1992.
(2) Brucher, E.; Glaser, J.; Toth, I. *Inorg. Chem.* **1991**, *30*, 2239−2241.
(3) Poinssot, C.; Geckeis, H. *Radionuclide Behavior in the Natural Environment; Science, Implications, and Lessons for the Nuclear Industry*; Woodhead Publishing Ltd.: Cambridge, U.K., 2012.
(4) Szabó, Z.; Toraishi, T.; Vallet, V.; Grenthe, I. *Coord. Chem. Rev.* **2006**, *250*, 784−815.
(5) Dozol, M.; Hagemann, R. *Pure Appl. Chem.* **1993**, *65*, 1081−1081.
(6) Novikov, A. *Geochem. Int.* **2010**, *48*, 1263−1387.
(7) Maher, K.; Bargar, J. R.; Brown, G. E., Jr. *Inorg. Chem.* **2012**, *52*, 3510−3532.
(8) Clark, D. L.; Conradson, S. D.; Donohoe, R. J.; Keogh, D. W.; Morris, D. E.; Palmer, P. D.; Rogers, R. D.; Tait, C. D. *Inorg. Chem.* **1999**, *38*, 1456−1466.
(9) Ikeda-Ohno, A.; Hennig, C.; Rossberg, A.; Funke, H.; Scheinost, A. C.; Bernhard, G.; Yaita, T. *Inorg. Chem.* **2008**, *47*, 8294−305.
(10) Shilov, V. P.; G., A. V.; Fedoseev, A. M. *Radiochemistry* **2012**, *54*, 212−227.
(11) Vasudeva Rao, P.; Gudi, N.; Bagawde, S.; Patil, S. *J. Inorg. Nucl. Chem.* **1979**, *41*, 235−239.
(12) Hindman, J. C.; Sullivan, J. C.; Cohen, D. *J. Am. Chem. Soc.* **1958**, *80*, 1812−1814.
(13) Rao, L.; Srinivasan, T. G.; Garnov, A. Y.; Zanonato, P.; Di Bernardo, P.; Bismondo, A. *Geochim. Cosmochim. Acta* **2004**, *68*, 4821−4830.
(14) Hindman, J.; Sullivan, J.; Cohen, D. *J. Am. Chem. Soc.* **1954**, *76*, 3278−3280.
(15) Rao, L.; Tian, G. *Symmetry* **2009**, *2*, 1−14.
(16) Clark, D. L.; Hobart, D. E.; Neu, M. P. *Chem. Rev.* **1995**, *95*, 25−48.
(17) Ikeda-Ohno, A.; Tsushima, S.; Takao, K.; Rossberg, A.; Funke, H.; Scheinost, A. C.; Bernhard, G.; Yaita, T.; Hennig, C. *Inorg. Chem.* **2009**, *48*, 11779−87.
(18) Maya, L. *Inorg. Chem.* **1983**, *22*, 2093−2095.
(19) Clark, D. L.; Hobart, D. E.; Palmer, P. D.; Sullivan, J. C.; Stout, B. E. *J. Alloys Compd.* **1993**, *193*, 94−97.
(20) Wester, D.; Sullivan, J. *J. Inorg. Nucl. Chem.* **1981**, *43*, 2919−2923.
(21) Grenthe, I.; Riglet, C.; Vitorge, P. *Inorg. Chem.* **1986**, *25*, 1679−1684.
(22) Maya, L. *Inorg. Chem.* **1982**, *21*, 2895−2898.
(23) Madic, C.; Hobart, D.; Begun, G. *Inorg. Chem.* **1983**, *22*, 1494−1503.
(24) Tait, C.; Palmer, P.; Ekberg, S.; Clark, D. *Report on neptunium speciation by NMR and optical spectroscopies*; Los Alamos National Lab.: Los Alamos, NM, 1995.
(25) Swift, T. J.; Connick, R. E. *J. Chem. Phys.* **1962**, *37*, 307−20.
(26) Harley, S. J.; Ohlin, C. A.; Casey, W. H. *Geochim. Cosmochim. Acta* **2011**, *75*, 3711−3725.
(27) Helm, L.; Nicolle, G. M.; Merbach, R. E. *Adv. Inorg. Chem.* **2005**, *57*, 327−379.

(28) Johnson, R. L.; Harley, S. J.; Ohlin, C. A.; Panasci, A. F.; Casey, W. H. *ChemPhysChem* **2011**, *12*, 2903−2906.
(29) Snow, M. S.; Zhao, P.; Dai, Z.; Kersting, A. B.; Zavarin, M. *J. Colloid Interface Sci.* **2013**, *390*, 176−182.
(30) Johnson, A.; Shepherd, G. *Spectrophotometry of neptunium in nitric acid solutions*; Dow Chemical Co.: Golden, CO, 1967.
(31) Sjoblom, R.; Hindman, J. *J. Am. Chem. Soc.* **1951**, *73*, 1744−1751.
(32) Hagan, P.; Cleveland, J. *J. Inorg. Nucl. Chem.* **1966**, *28*, 2905−2909.
(33) Ammann, C.; Meier, P.; Merbach, A. *J. Magn. Reson.* **1982**, *46*, 319−321.
(34) Kaplan, M.; Bovey, F.; Cheng, H. *Anal. Chem.* **1975**, *47*, 1703−1705.
(35) Mizuoka, K.; Grenthe, I.; Ikeda, Y. *Inorg. Chem.* **2005**, *44*, 4472−4474.
(36) Szabó, Z.; Grenthe, I. *Inorg. Chem.* **2010**, *49*, 4928−4933.
(37) Banyai, I.; Glaser, J.; Micskei, K.; Toth, I.; Zekany, L. *Inorg. Chem.* **1995**, *34*, 3785−3796.
(38) Deglint, E.; Martens, H.; Edwards, E.; Boon, N.; Dance, P.; Weinberg, N. *Phys. Chem. Chem. Phys.* **2011**, *13*, 438−440.